Journal of Mathematical Modeling
Vol. -, No. -, 2026, pp. -. Research Article

JMM

Blood flow through a stenosed artery under MHD two-phase conditions with Hall effect, radiation and diffusion

Surendra Kumar Agarwal[†*], **Gauri Sethi**[†], **Astha Pareek**[‡]

[†]*Department of Mathematics, IIS (Deemed to be University), Jaipur, India*
[‡]*Department of Computer Science, IIS (Deemed to be University), Jaipur, India*
Email(s): surendrakumar.agarwal@iisuniv.ac.in, gaurisethi36320@iisuniv.ac.in, astha.pareek@iisuniv.ac.in

Abstract. This study investigates the combined effects of heat and mass transfer on two-phase blood flow through a stenosed artery, considering the influence of the Hall current. Blood is modeled as a Newtonian fluid in both the central core and plasma regions. A system of differential equations governing momentum, temperature, and concentration is developed separately for each region. The analysis incorporates magnetic field, thermal radiation, and Hall current effects. Key flow characteristics, including flow resistance, total volumetric flow rate, and wall shear stress, are evaluated for varying magnetic field strengths, radiation parameters, and Hall current intensities. The findings indicate that stronger magnetic fields and radiation levels lead to a reduction in blood flow velocity and temperature. The inclusion of the Hall current introduces a cross-flow component due to the induced electric field, further modifying the velocity distribution, particularly in the plasma region. Moreover, an increase in the Schmidt number enhances the concentration profiles in both the core and plasma regions. Overall, the Hall effect significantly alters the magnetic interaction with the flow, impacting the distribution of mechanical and thermal quantities throughout the arterial segment. The results have potential biomedical applications in magnetic resonance imaging (MRI), targeted drug delivery, and electromagnetic therapy, where controlled magnetic and electric fields influence blood flow and heat transfer in vascular systems.

Keywords: Blood flow, lorentz force, artery, stenosis, heat-mass transfer.
AMS Subject Classification 2020: 34B15, 76W05, 92-10.

1 Introduction

In the last decades, a significant interest has been focused on the examination of blood flow as a two-phase fluid, where the blood has a core region of red blood cells and an encompassing layer of plasma.

*Corresponding author
Received: 01 September 2025/ Revised: 04 November 2025/ Accepted: 29 November 2025
DOI: 10.22124/jmm.2025.31551.2840

This dual-layered architecture has a strong impact on hemodynamics, notably flow resistance, nutrient transport (diffusion) and shear stress. Stenosis refers the abnormal and unnatural growth of the arterial wall thickness at certain sites of the circulatory system under the diseased states, which sometimes leads to the fatal circumstances. Magnetohydrodynamics (MHD) is the study that considers these effects with Lorentz force that arises from the induced electric and magnetic fields. The basics of MHD are closely related to human blood flow especially to medical imaging devices (like MRI) where applied magnetic fields would take the place of electrically conducting blood movement. The mathematical study of blood flow and the complex dynamics that govern it, by nature, has been modeled both analytically and computationally by multiple mathematicians in the past.

Haik et al. [6] proposed a mathematical model based on Ferrohydrodynamics (FHD), with the assumptions that there is no induced electric current and that the flow of the fluid is only due to the magnetization of the fluid in the applied magnetic field. Ogulu et al. [8] studied the effect of heat transfer on blood flow through a stenosed artery under the assumption of an optically thin fluid. They found that heat transfer modifies the velocity and temperature profiles along with stenosis and magnetic field, as would be the case in a feverish patient.

Sankar et al. [10] evaluated pulsatile two-phase blood flow through a stenosed artery by modeling the core blood phase as a coroidal-Bulkley fluid and the peripheral plasma as a Newtonian fluid. They found the plug core radius and resistance for the plug flow section increased with stenosis size, while K_n and N increased with increasing wall shear stress. Ellahi et al. [3]studied the unsteady incompressible flow of non-Newtonian fluids through constricted arterial segments using a micropolar fluid model. The effects of slip velocity and mild stenosis for better representation of blood flow behaviour were also included in their analysis. Expressions for velocity and volumetric flow rate were derived using modified Bessel functions.

Garcia et al. [4] studied the effects of heat transfer while evaluating two-phase blood flow through a stenosed artery with viscous heating. Their findings indicated that the heat generated as a result of viscous effects is enough to raise blood temperatures above that of the arterial wall temperatures. The study by Sharma et al. [12] investigated the effect of an external magnetic field on blood flow through a model of artificial blood that contains magnetic particles using an MHD-based model. Numerical as well as experimental data indicated that increasing magnetic field strength results in decreased velocity.

Agarwal et al. [1] examined the two-dimensional laminar boundary layer flow of a viscous, incompressible fluid over a porous heated plate moving vertically. The Natural Transform Technique was employed to analyze the effects of various parameters. The authors showed that the values of the parameters had a big effect on velocity, temperature distribution, heat transfer rate, and skin friction. Tripathi et al. [18] investigated the effects of heat and mass transfer on two-phase blood flow through a stenosed artery in the presence of an external magnetic field and thermal radiation, considering the pulsatile nature of the flow. Blood, being an electrically conducting fluid, is notably influenced by external magnetic fields.

Khandelwal et al. [7] studied the phenomenon of heat transfer in a pipe in a Hagen-Poiseuille flow on the axial heat conduction and temperature gradients for multiple fluids. Hydrogen and air behaved differently with exponential temperature, and all fluids behaved similarly with sinusoidal temperature.

Sethi et al. [11] modeled Jeffrey fluid flow in a catheterized curved stenosed artery affected by magnetic, thermal, and mass transfer parameters. The authors observed that the stenosis height, slip, catheter radius, and Hartmann number influenced flow response.

Recent investigations [2,5,13–17] have shown that MHD nanofluid flows through porous or bounded

channels are greatly affected by magnetic field strength, Hall current, and induced magnetic effects. Variations in nanoparticle concentration, wall conductivity, and magnetic interaction parameters significantly alter the velocity, temperature, and heat transfer characteristics of the fluid. In the context of biomedical transport, such as blood flow in magnetized arteries, Joule heating and viscous dissipation enhance thermal energy distribution, whereas magnetic drag tends to suppress flow motion.

The present work builds on previous investigations of heat and mass transfer in stenosed arteries by including Hall currents in a two-phase blood flow model, assuming blood is a Newtonian fluid in both the core and plasma regions, and observing the effects of the magnetic field, thermal radiation, and Hall current. This study has shown that the magnetic, thermal, and flow parameters critically affect blood-nanoparticle interactions in stenosed arteries with respect to velocity, drug delivery, and thermal regulation. The study findings provide insights as we move towards advanced magnetic drug targeting, enhanced diagnostics, and management of vascular disease.

2 Mathematical formulation

Let us assume the artery is aligned horizontally along the x-axis and the flow is in the axial direction (Figure 1). Blood flow through a vessel is modeled using a two phase model in which the central core of the vessel $\bar{R}_c(\bar{x})$ is occupied by a spatially homogeneous suspension of red blood cells, or hematocrit, and $\bar{R}_p(\bar{x})$ is surrounded by a plasma layer. This system is passed in a narrowed cylindrical artery of radius $\bar{R}_n$. The flow is under the presence of external magnetic field, Hall current and thermal radiation. The flow direction is perpendicular to the magnetic field. The viscosities for the core and plasma regions are taken as [9]

$$\bar{\mu}(r) = \begin{cases} \bar{\mu}_c & \text{for } 0 \le r \le \bar{R}_1(\bar{x}), \\ \bar{\mu}_p & \text{for } \bar{R}_1(x) \le r \le \bar{R}_n(\bar{x}). \end{cases}$$

The model of the geometry of the stenosis in the plasma and core regions is defined separately to reflect the layered structure of the artery as follows:

$$\bar{R}_p(\bar{x}) = \begin{cases} 1 - h_{p_0}\left[1 - \cos\left(\dfrac{2\pi(x-x_0)}{L_s}\right)\right], & x_0 \le x \le x_0 + L_s \\ 1, & \text{otherwise} \end{cases} \tag{1}$$

$$\bar{R}_c(\bar{x}) = \begin{cases} R_{c_0}\left[1 - h_c\, e^{-\varepsilon(x-x_c)^2} \sin^2\left(\dfrac{\pi(x-x_c)}{L_s}\right)\right], & |x-x_c| \le \dfrac{L_s}{2} \\ R_{c_0}, & \text{otherwise} \end{cases} \tag{2}$$

The geometry of the plasma region $\bar{R}_p(\bar{x})$ represents a smooth and symmetric narrowing of the arterial wall using a cosine profile within the stenosis length $[x_0, x_0 + L_s]$, while remains constant elsewhere. The geometry of the core region $\bar{R}_c(\bar{x})$ models a localized narrowing of the central core using a Gaussian-modulated sine-square function centered at x_c, with a constant radius outside the stenosed area.

Under the above assumptions, the governing equations for momentum, energy, and concentration in the core region of the artery are formulated as

$$\bar{\mathbf{d}}_c \frac{\partial \bar{w}_c}{\partial \bar{t}_e} = -\frac{\partial \bar{p}_0}{\partial \bar{x}} + \bar{\mu}_c \left(\frac{\partial^2 \bar{w}_c}{\partial \bar{r}^2} + \frac{1}{\bar{r}}\frac{\partial \bar{w}_c}{\partial \bar{r}}\right) - \bar{\sigma}\bar{B}^2 \bar{w}_c, \tag{3}$$

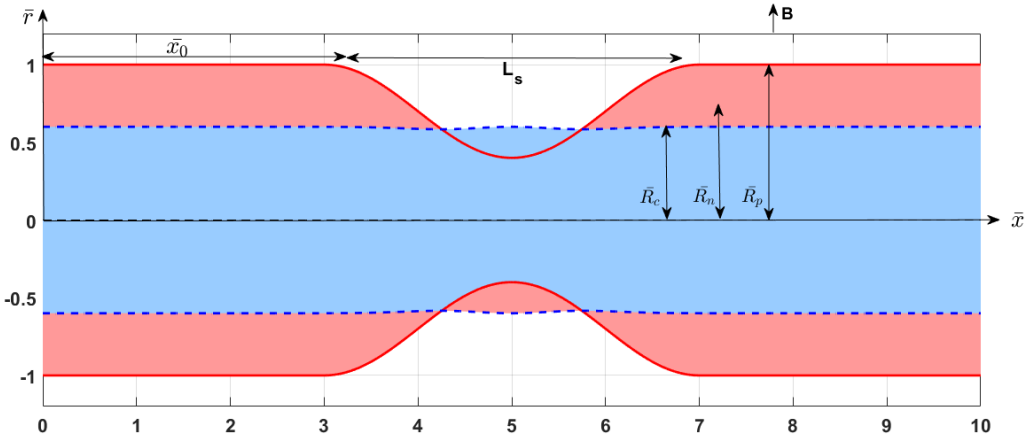

Figure 1: Schematic diagram of core and plasma regions

$$\bar{\mathbf{d}}_c \bar{c}_c \frac{\partial \bar{\Theta}_c}{\partial \bar{t}_e} = \bar{K}_c \left(\frac{\partial^2 \bar{\Theta}_c}{\partial \bar{r}^2} + \frac{1}{\bar{r}} \frac{\partial \bar{\Theta}_c}{\partial \bar{r}} \right) - \frac{\partial \bar{q}_c}{\partial \bar{r}}, \tag{4}$$

$$\frac{\partial \bar{C}_c}{\partial \bar{t}_e} = \bar{D}_c \left(\frac{\partial^2 \bar{C}_c}{\partial \bar{r}^2} + \frac{1}{\bar{r}} \frac{\partial \bar{C}_c}{\partial \bar{r}} \right). \tag{5}$$

In the same manner,the governing equations for Momentum, Energy and Concentration in plasma region are

$$\bar{\mathbf{d}}_p \frac{\partial \bar{w}_p}{\partial \bar{t}_e} = -\frac{\partial \bar{p}_0}{\partial \bar{x}} + \bar{\mu}_p \left(\frac{\partial^2 \bar{w}_p}{\partial \bar{r}^2} + \frac{1}{\bar{r}} \frac{\partial \bar{w}_p}{\partial \bar{r}} \right) - \frac{\bar{\sigma} \bar{B}^2 \bar{w}_p}{1 + m_h^2}, \tag{6}$$

$$\bar{\mathbf{d}}_p \bar{c}_p \frac{\partial \bar{\Theta}_p}{\partial \bar{t}_e} = \bar{K}_p \left(\frac{\partial^2 \bar{\Theta}_p}{\partial \bar{r}^2} + \frac{1}{\bar{r}} \frac{\partial \bar{\Theta}_p}{\partial \bar{r}} \right) - \frac{\partial \bar{q}_p}{\partial \bar{r}}, \tag{7}$$

$$\frac{\partial \bar{C}_p}{\partial \bar{t}_e} = \bar{D}_p \left(\frac{\partial^2 \bar{C}_p}{\partial \bar{r}^2} + \frac{1}{\bar{r}} \frac{\partial \bar{C}_p}{\partial \bar{r}} \right). \tag{8}$$

The subscripts in the formulas stand for parameters unique to the plasma (p) and core (c) areas of blood flow. The pressure gradient $\frac{\partial \bar{p}_0}{\partial \bar{x}}$ along the artery, the electrical conductivity $\bar{\sigma}$ of blood, and the impact of an external magnetic field B_0 are all taken into account in the model. Additionally, the effect of Hall current, which arises due to the interaction between the magnetic field and induced electric field, is incorporated to better represent the behavior of electrically conducting blood under magnetic influence. Important physical characteristics including mass diffusivity $\bar{D}_b$, density, s_0 specific heat, and thermal conductivity $\bar{K}_b$ are also included. The three main flow variables are concentration $\bar{C}$, temperature $\bar{\Theta}$, and velocity $\bar{w}$. Thermal radiation's $\frac{\partial \bar{q}_p}{\partial \bar{r}}$ and $\frac{\partial \bar{q}_c}{\partial \bar{r}}$ impact on heat transfer in the blood flow is also represented by the radiation-related factors in the energy equations for both regions as follows:

$$\frac{\partial \bar{q}_p}{\partial \bar{r}} = 4\bar{\gamma}_p^2(\bar{\Theta}_p - \bar{\Theta}_0), \frac{\partial \bar{q}_c}{\partial \bar{r}} = 4\bar{\gamma}_c^2(\bar{\Theta}_c - \bar{\Theta}_0).$$

It is interesting to note that both core and plasma behave as optically thin fluids with relatively low densities under physiological conditions. Because of this, research generally indicates that the mean

radiation absorption coefficients for the core $\bar{\gamma}_c$ and plasma $\bar{\gamma}_p$ areas are roughly equal to one [7], that is $\bar{\gamma}_c \sim \bar{\gamma}_p \approx 1$.

Boundary Conditions are

$$\begin{cases} \bar{w}_p = 0, \quad \bar{\Theta}_p = \bar{\Theta}_w, \quad \bar{C}_p = \bar{C}_w & \text{at } \bar{r} = \bar{R}_p(\bar{x}), \\ \bar{w}_c = \bar{w}_p, \quad \bar{\Theta}_p = \bar{\Theta}_c, \quad \bar{C}_p = \bar{C}_c, \quad \bar{\tau}_c = \bar{\tau}_p, \quad \dfrac{\partial \bar{\Theta}_c}{\partial \bar{r}} = \dfrac{\partial \bar{\Theta}_p}{\partial \bar{r}}, \quad \dfrac{\partial \bar{C}_c}{\partial \bar{r}} = \dfrac{\partial \bar{C}_p}{\partial \bar{r}} & \text{at } \bar{r} = \bar{R}_c(\bar{x}), \\ \dfrac{\partial \bar{w}_c}{\partial \bar{r}} = 0, \quad \dfrac{\partial \bar{\Theta}_c}{\partial \bar{r}} = 0, \quad \dfrac{\partial \bar{C}_c}{\partial \bar{r}} = 0 & \text{at } \bar{r} = 0. \end{cases}$$

To expand the model and examine the relative impacts of physical characteristics on blood flow, dimensionless variables are employed:

$$w_c = \frac{\bar{w}_c}{\bar{w}_0}, \quad r = \frac{\bar{r}}{\bar{R}_n}, \quad x = \frac{\bar{x}}{\bar{R}_n}, \quad \bar{f}_b = \frac{\bar{t}_e}{t_e}, \quad R(x) = \frac{\bar{R}(\bar{x})}{\bar{R}_n}, \quad p_0 = \frac{\bar{R}_n \bar{p}_0}{\bar{w}_0 \bar{\mu}_p}, \quad h = \frac{\bar{h}_s}{\bar{R}_n},$$

$$D_b = \frac{\bar{D}_p}{\bar{D}_c}, \quad R_{ey} = \frac{\bar{\mathbf{d}}_p \bar{R}_n^2 \bar{f}_b}{\bar{\mu}_p}, \quad \theta_c = \frac{\bar{\Theta}_c - \bar{\Theta}_0}{\bar{\Theta}_w - \bar{\Theta}_0}, \quad a_c = \frac{\bar{C}_c - \bar{C}_0}{\bar{C}_w - \bar{C}_0}, \quad w_p = \frac{\bar{w}_p}{\bar{w}_0},$$

$$\theta_p = \frac{\bar{\Theta}_p - \bar{\Theta}_0}{\bar{\Theta}_w - \bar{\Theta}_0}, \quad a_p = \frac{\bar{C}_p - \bar{C}_0}{\bar{C}_w - \bar{C}_0}, \quad \mu_b = \frac{\bar{\mu}_p}{\bar{\mu}_c}, \quad R_d^2 = \frac{4\bar{R}_n^2 \bar{\gamma}_p^2}{\bar{K}_p}, \quad H_a^2 = \frac{\sigma \bar{B}^2 \bar{R}_n^2}{\bar{\mu}_p},$$

$$P_e = \frac{\bar{\mathbf{d}}_p \bar{c}_p \bar{R}_n^2 \bar{f}_b}{\bar{K}_p}, \quad S_c = \frac{\bar{\mu}_p}{\bar{D}_p \bar{\mathbf{d}}_p}, \quad \mathbf{d}_b = \frac{\bar{\mathbf{d}}_p}{\bar{\mathbf{d}}_c}, \quad K_b = \frac{\bar{K}_p}{\bar{K}_c}, \quad s_0 = \frac{\bar{s}_p}{\bar{s}_c}, \quad \gamma_b = \frac{\bar{\gamma}_p}{\bar{\gamma}_c}.$$

Therefore above equations of both core and plasma regions in non dimensional form can be represented as :

Core Region Equations:

$$\left(\frac{R_{ey}}{\mathbf{d}_b}\right) \frac{\partial w_c}{\partial t_e} = -\frac{\partial p_0}{\partial x} + \frac{1}{\mu_b}\left(\frac{\partial^2 w_c}{\partial r^2} + \frac{1}{r}\frac{\partial w_c}{\partial r}\right) - H_a^2 w_c, \tag{9}$$

$$\frac{P_e K_0}{\mathbf{d}_b s_0} \frac{\partial \theta_c}{\partial t_e} = \left(\frac{\partial^2 \theta_c}{\partial r^2} + \frac{1}{r}\frac{\partial \theta_c}{\partial r}\right) - \frac{K_0}{\gamma_b^2} R_d^2 \theta_c, \tag{10}$$

$$R_{ey}\left(\frac{\partial a_c}{\partial t_e}\right) = \frac{1}{D_b}\left(\frac{1}{S_c}\right)\left(\frac{\partial^2 a_c}{\partial r^2} + \frac{1}{r}\frac{\partial a_c}{\partial r}\right). \tag{11}$$

Plasma Region Equations:

$$R_{ey}\frac{\partial w_p}{\partial t_e} = -\frac{\partial p_0}{\partial x} + \left(\frac{\partial^2 w_p}{\partial r^2} + \frac{1}{r}\frac{\partial w_p}{\partial r}\right) - \frac{H_a^2 w_p}{1 + m_h^2}, \tag{12}$$

$$P_e \frac{\partial \theta_p}{\partial t_e} = \left(\frac{\partial^2 \theta_p}{\partial r^2} + \frac{1}{r}\frac{\partial \theta_p}{\partial r}\right) - R_d^2 \theta_p, \tag{13}$$

$$R_{ey}\left(\frac{\partial a_p}{\partial t_e}\right) = \left(\frac{1}{S_c}\right)\left(\frac{\partial^2 a_p}{\partial r^2} + \frac{1}{r}\frac{\partial a_p}{\partial r}\right). \tag{14}$$

Boundary Conditions:

$$\begin{cases} w_p = 0, \quad \theta_p = 1, \quad a_p = 1 & \text{at } r = R_p(x), \\ w_p = w_c, \quad \theta_p = \theta_c, \quad a_p = a_c, \quad \tau_c = \tau_p, \quad \frac{\partial \theta_c}{\partial r} = \frac{\partial \theta_p}{\partial r}, \quad \frac{\partial a_c}{\partial r} = \frac{\partial a_p}{\partial r} & \text{at } r = R_c(x), \\ \frac{\partial w_c}{\partial r} = 0, \quad \frac{\partial \theta_c}{\partial r} = 0, \quad \frac{\partial a_c}{\partial r} = 0 & \text{at } r = 0. \end{cases}$$

To solve the above system of equations, first we use the separation of variables method:

$$-\frac{\partial p_0}{\partial x} = P_0 e^{i\omega t_e}, \quad w_c(r,t_e) = w_{c_0}(r)e^{i\omega t_e}, \quad w_p(r,t_e) = w_{p_0}(r)e^{i\omega t_e},$$

$$\theta_c(r,t_e) = \theta_{c_0}(r)e^{i\omega t_e}, \quad \theta_p(r,t_e) = \theta_{p_0}(r)e^{i\omega t_e}, \quad a_c(r,t_e) = a_{c_0}(r)e^{i\omega t_e}, \quad a_p(r,t_e) = a_{p_0}(r)e^{i\omega t_e}.$$

Using the appropriate assumptions and boundary conditions, the governing equations reduce to the following forms in the core and plasma regions:

$$\left(\frac{\partial^2 w_{c_0}}{\partial r^2} + \frac{1}{r}\frac{\partial w_{c_0}}{\partial r}\right) - \left(H_a^2 + \frac{R_{ey}}{\mathbf{d}_b} i\omega\right) \mu_b w_{c_0} = -P_0 \mu_b, \tag{15}$$

$$\frac{\partial^2 \theta_{c_0}}{\partial r^2} + \frac{1}{r}\frac{\partial \theta_{c_0}}{\partial r} - \left(\frac{K_0 R_d^2}{\gamma_b^2} + i\omega \frac{P_e}{\mathbf{d}_b}\frac{K_0}{s_0}\right) \theta_{c_0} = 0, \tag{16}$$

$$\frac{\partial^2 a_{c_0}}{\partial r^2} + \frac{1}{r}\frac{\partial a_{c_0}}{\partial r} - (i\omega R_{ey} D_b S_c)\, a_{c_0} = 0. \tag{17}$$

Under suitable assumptions, the governing differential equations reduce to modified Bessel equations:

$$\left(\frac{\partial^2 w_{c_0}}{\partial r^2} + \frac{1}{r}\frac{\partial w_{c_0}}{\partial r}\right) - \lambda_1 w_{c_0} = -P_0 \mu_b, \tag{18}$$

$$\frac{\partial^2 \theta_{c_0}}{\partial r^2} + \frac{1}{r}\frac{\partial \theta_{c_0}}{\partial r} - \beta_1 \theta_{c_0} = 0, \tag{19}$$

$$\frac{\partial^2 a_{c_0}}{\partial r^2} + \frac{1}{r}\frac{\partial a_{c_0}}{\partial r} - \xi_1 a_{c_0} = 0. \tag{20}$$

These are solved analytically to obtain the expressions for velocity, temperature, and concentration:

$$w_{c_0}(r) = C_1 J_0(\sqrt{\lambda_1} r) + C_2 Y_0(\sqrt{\lambda_1} r) + A_1 J_0(\sqrt{\lambda_1} r) + B_1 Y_0(\sqrt{\lambda_1} r) \tag{21}$$

$$\theta_c(r,t_e) = \left[\left(\frac{\sqrt{\beta_2} Y_1(\sqrt{\beta_2} R_c)}{V_3 Y_0(\sqrt{\beta_2} R_p)} - \frac{\sqrt{\beta_1} V_2 J_1(\sqrt{\beta_1} R_c)}{V_3}\right) V_1 + V_2\right] J_0(\sqrt{\beta_1} r) e^{i\omega t_e} \tag{22}$$

$$a_c(r,t_e) = \left[\left(\frac{\sqrt{\xi_2} Y_1(\sqrt{\xi_2} R_c)}{V_6 Y_0(\sqrt{\xi_2} R_p)} - \frac{\sqrt{\xi_1} V_5 J_1(\sqrt{\xi_1} R_c)}{V_6}\right) V_4 + V_5\right] J_0(\sqrt{\xi_1} r) e^{i\omega t_e} \tag{23}$$

See Appendix 1 for the values of constants used.

Similarly, in the plasma region

$$\left(\frac{\partial^2 w_{p_0}}{\partial r^2}+\frac{1}{r}\frac{\partial w_{p_0}}{\partial r}\right)-\left(\frac{H_a^2}{1+m_h^2}+R_{ey}i\omega\right)w_{p_0}=-P_0, \tag{24}$$

$$\frac{\partial^2 \theta_{p_0}}{\partial r^2}+\frac{1}{r}\frac{\partial \theta_{p_0}}{\partial r}-\left(R_d^2+i\omega P_e\right)\theta_{p_0}=0, \tag{25}$$

$$\frac{\partial^2 a_{p_0}}{\partial r^2}+\frac{1}{r}\frac{\partial a_{p_0}}{\partial r}-i\omega R_{ey}S_c a_{p_0}=0. \tag{26}$$

The corresponding set of equations in Bessel's form are as follows:

$$\frac{\partial^2 w_{p_0}}{\partial r^2}+\frac{1}{r}\frac{\partial w_{p_0}}{\partial r}-\lambda_2 w_{p_0}=-P_0, \tag{27}$$

$$\frac{\partial^2 \theta_{p_0}}{\partial r^2}+\frac{1}{r}\frac{\partial \theta_{p_0}}{\partial r}-\beta_2\theta_{p_0}=0, \tag{28}$$

$$\frac{\partial^2 a_{p_0}}{\partial r^2}+\frac{1}{r}\frac{\partial a_{p_0}}{\partial r}-\xi_2 a_{p_0}=0. \tag{29}$$

Analytical solutions are obtained for the velocity, temperature, and concentration distributions for plasma region as follows:

$$w_{p_0}(r)=C_3J_0(\sqrt{\lambda_2}r)+C_4Y_0(\sqrt{\lambda_2}r)+A_2J_0(\sqrt{\lambda_2}r)+B_2Y_0(\sqrt{\lambda_2}r), \tag{30}$$

$$\theta_p(r,t_e)=\left[\left(\frac{\sqrt{\beta_2}Y_1(\sqrt{\beta_2}R_c)}{V_3\,Y_0(\sqrt{\beta_2}R_p)}-\frac{\sqrt{\beta_1}V_2J_1(\sqrt{\beta_1}R_c)}{V_3}\right)\left(J_0(\sqrt{\beta_2}r)-\frac{J_0(\sqrt{\beta_2}R_p)}{Y_0(\sqrt{\beta_2}R_p)}Y_0(\sqrt{\beta_2}r)\right)+\frac{Y_0(\sqrt{\beta_2}r)}{Y_0(\sqrt{\beta_2}R_p)}\right]e^{i\omega t_e} \tag{31}$$

$$a_p(r,t_e)=\left[\left(\frac{\sqrt{\xi_2}Y_1(\sqrt{\xi_2}R_c)}{V_6\,Y_0(\sqrt{\xi_2}R_p)}-\frac{\sqrt{\xi_1}V_5J_1(\sqrt{\xi_1}R_c)}{V_6}\right)\left(J_0(\sqrt{\xi_2}r)-\frac{J_0(\sqrt{\xi_2}R_p)}{Y_0(\sqrt{\xi_2}R_p)}Y_0(\sqrt{\xi_2}r)\right)+\frac{Y_0(\sqrt{\xi_2}r)}{Y_0(\sqrt{\xi_2}R_p)}\right]e^{i\omega t_e} \tag{32}$$

The velocity equations, being nonhomogeneous, are solved using the method of variation of parameters. The general solutions are combinations of homogeneous solutions involving Bessel functions J_0 and Y_0, and particular integrals. Constants used emerge from the particular solution process and are expressed in terms of system parameters and source terms in Appendix 1.

The fluid flow rate is

$$F_{total}=2\pi R_p^2\int_0^{R_c}w_c(r,t_e)\,dr+2\pi R_p^2\int_{R_c}^{R_p}w_p(r,t_e)\,dr$$

$$= 2\pi R_p^2 \Bigg\{ \frac{1}{\sqrt{\lambda_1}} \Big[(C_1 + A_1) J_1(\sqrt{\lambda_1} R_c) + (C_2 + B_1) Y_1(\sqrt{\lambda_1} R_c) \Big] + \frac{1}{\sqrt{\lambda_2}} \Big[(C_3 + A_2) \big(J_1(\sqrt{\lambda_2} R_p) - J_1(\sqrt{\lambda_2} R_c) \big) + (C_4 + B_2) \big(Y_1(\sqrt{\lambda_2} R_p) - Y_1(\sqrt{\lambda_2} R_c) \big) \Big] \Bigg\}.$$

The expression for impedance is

$$Z = \frac{P_0 e^{i\omega t_e}}{F_{total}} = \frac{P_0 e^{i\omega t_e}}{2\pi R_p^2} \Bigg[\frac{1}{\sqrt{\lambda_1}} \Big((C_1 + A_1) J_1(\sqrt{\lambda_1} R_c) + (C_2 + B_1) Y_1(\sqrt{\lambda_1} R_c) \Big) + \frac{1}{\sqrt{\lambda_2}} \Big((C_3 + A_2) \left[J_1(\sqrt{\lambda_2} R_p) - J_1(\sqrt{\lambda_2} R_c) \right] + (C_4 + B_2) \left[Y_1(\sqrt{\lambda_2} R_p) - Y_1(\sqrt{\lambda_2} R_c) \right] \Big) \Bigg]^{-1}.$$

The wall shear stress is

$$\tau_b = \frac{1}{\mu_b} \left(\frac{\partial w_{p0}}{\partial r} \right)_{r=R_p} = -\frac{\sqrt{\lambda_2}}{\mu_b} \Big[(C_3 + A_2) J_1(\sqrt{\lambda_2} R_p) + (C_4 + B_2) Y_1(\sqrt{\lambda_2} R_p) \Big].$$

3 Numerical experiments

The results of this study are illustrated through various graphs, based on which the following observations are made. The velocity decreases in both the core and plasma regions with an increase in the Hartmann number (Figure 2), suggesting that the flow is damped by the magnetic field due to the Lorentz force opposing motion. Physically, this signifies that a stronger magnetic field can effectively control or slow down blood flow, which is useful in magnetically guided drug delivery, magnetotherapy, and regulation of blood motion in biomedical applications.

In the plasma region, velocity decreases with increasing Hall parameter (see Figure 3) because the Hall current diverts the induced current away from the axial direction. This reduces the axial component of the Lorentz force, which in turn weakens the driving force for fluid motion, leading to a lower velocity.

From Figure 4, we observed that the temperature in the flow field decreases with an increase in the radiation parameter. This trend indicates as the radiation parameter gets larger, the thermal radiation effect enhances energy loss from the fluid, thus, decreasing the temperature.

An increase in the Schmidt number is characterized by an increase in the concentration of the diffusing species. A higher Schmidt number is associated with lower mass diffusivity, which often results in steeper concentration gradients and higher concentrations local to the source (Figure 5). An increase in the radiation parameter decreases temperature, indicating better thermal management, while a higher Schmidt number increases concentration, relevant for diffusion and mass transfer analysis.

The volumetric flux is shown to decrease with an increase in the Reynolds number (Figure 6). This implies that large inertial forces compared to viscous forces oppose the development of a steady flow and decrease the net volumetric flow. Furthermore, the Reynolds number reduces volumetric flow rate, and increased stenosis height lowers wall shear stress, highlighting their importance in understanding hemodynamic behavior and plaque formation in arterial flow.

As the Hall parameter increases, the flow rate increases (Figure 7). The Hall effect changes the direction of the induced current. This means that the opposing Lorentz force is minimized in the axial direction, which reduces resistance to flow. When the resistance to flow decreases, the fluid flows more freely, causing an increase in the flow rate.

In Figure 8, impedance goes up as the Hartmann number increases, as a stronger magnetic field creates more magnetic resistance in the fluid, restricting the flow of the fluid. Efforts to maintain the same flow rate will require more pressure, resulting in more impedance.

The wall shear stress falls with an increase in stenosis height (Figure 9). A taller stenosis reduces the artery less than a shallower stenosis which has the effect of reducing the effective flow area of the artery, and altering the velocity gradient near the wall. This reduced velocity gradient causes a reduced shear force on the wall.

A higher Hall parameter produces a higher wall shear stress (Figure 10). This is because modified electromagnetic interactions with the Hall effect increase the velocity of the fluid next to the vessel wall, which results in an increased rate of shear and greater stress on the wall surface.

The streamline plots shown in the Figure 11, represent the flow behavior of blood through a stenosed artery with a catheter inserted, for three different stenosis severities: 10, 20, and 30 percent. The streamlines illustrate the path followed by blood particles and how the narrowing of the artery due to stenosis affects the flow field. As stenosis severity increases, streamlines become more compressed and distorted near the narrowed region, indicating stronger velocity gradients and flow disturbances. This visualization is part of a study investigating the hemodynamic behavior in a catheterized, stenosed artery under varying blockage levels, relevant to cardiovascular diagnostics and treatment modeling.

Typically, the magnetic field strength in biomedical applications ranges between 0.1–2 T, which corresponds to fields used in MRI and magnetic drug targeting. The Hall parameter and radiation parameter values considered fall within physiologically acceptable limits to ensure realistic modeling of blood flow and heat transfer. These parameter ranges reflect conditions encountered in clinical or therapeutic environments, thereby enhancing the biomedical relevance and applicability of the present study.

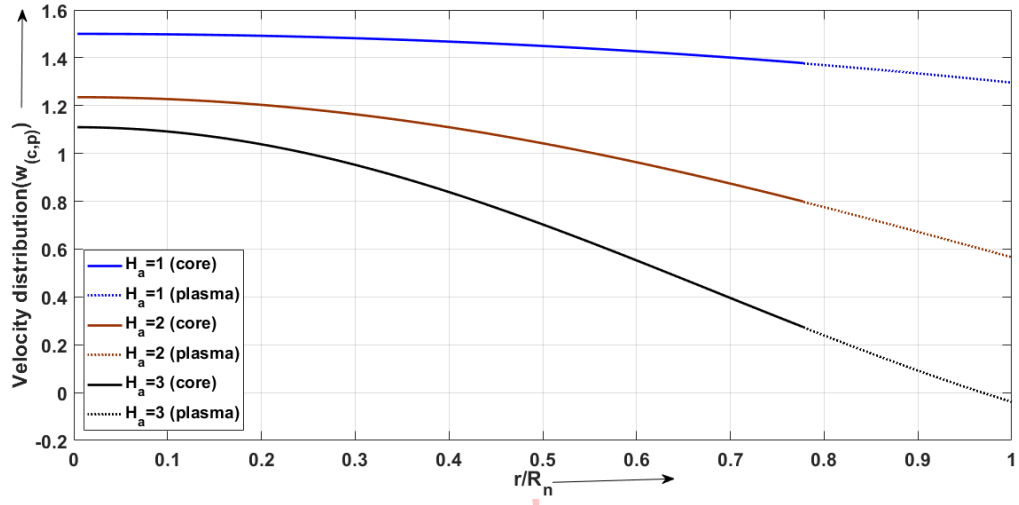

Figure 2: The effect of Hartmann number on velocity distribution

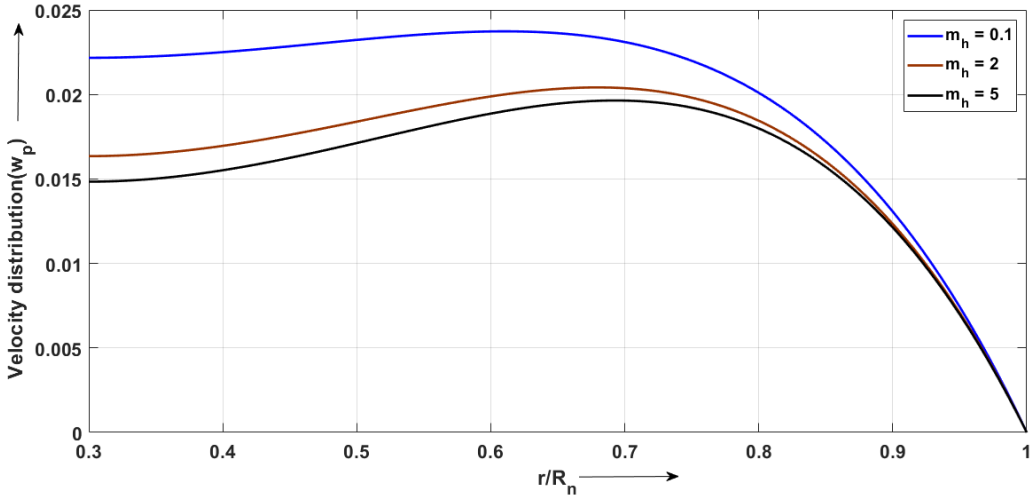

Figure 3: The effect of Hall parameter on velocity distribution

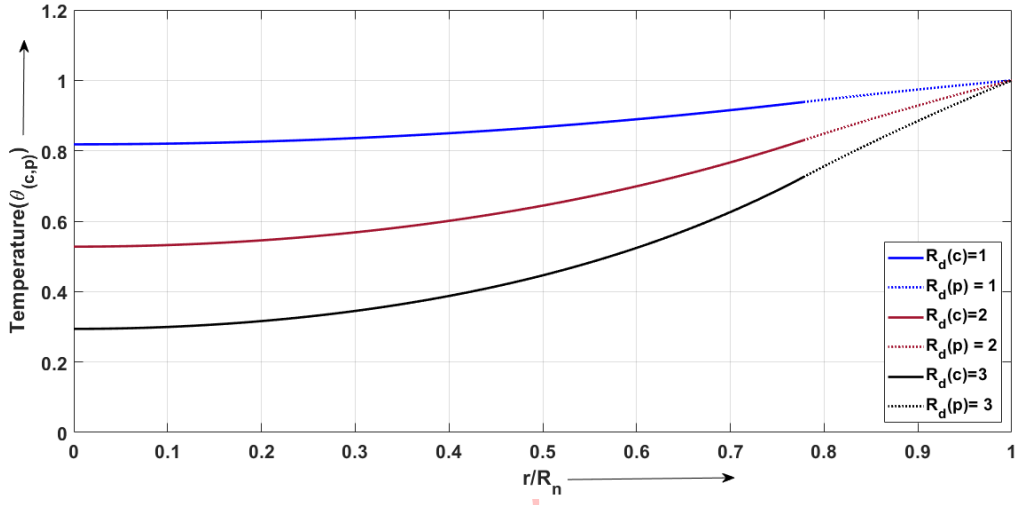

Figure 4: The effect of radiation parameter on temperature

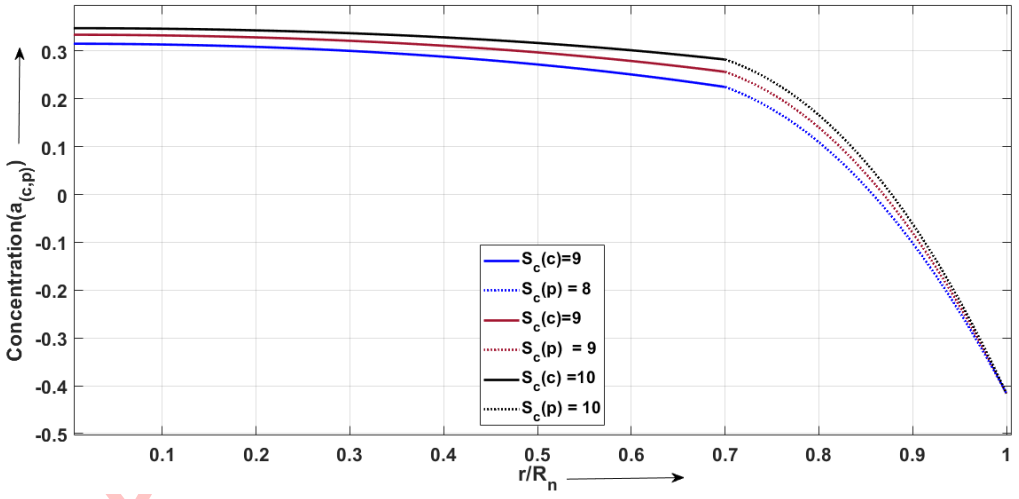

Figure 5: The effect of Schmidt number on concentration

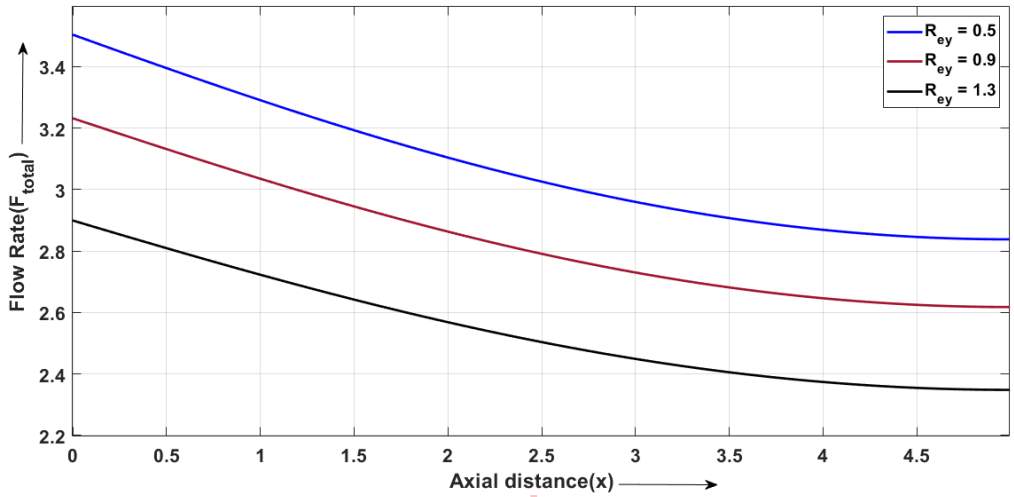

Figure 6: The effect of Reynolds number on flow rate

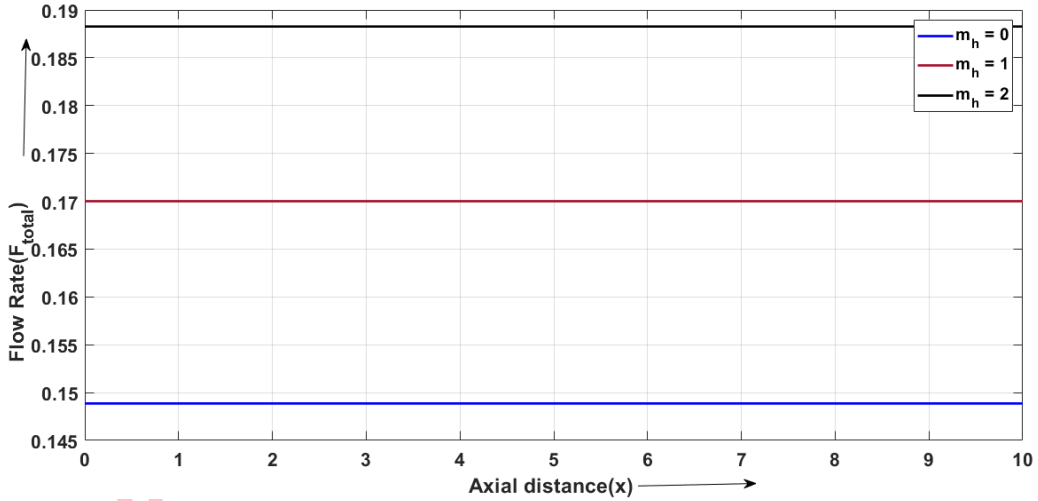

Figure 7: The effect of Hall parameter on flow rate

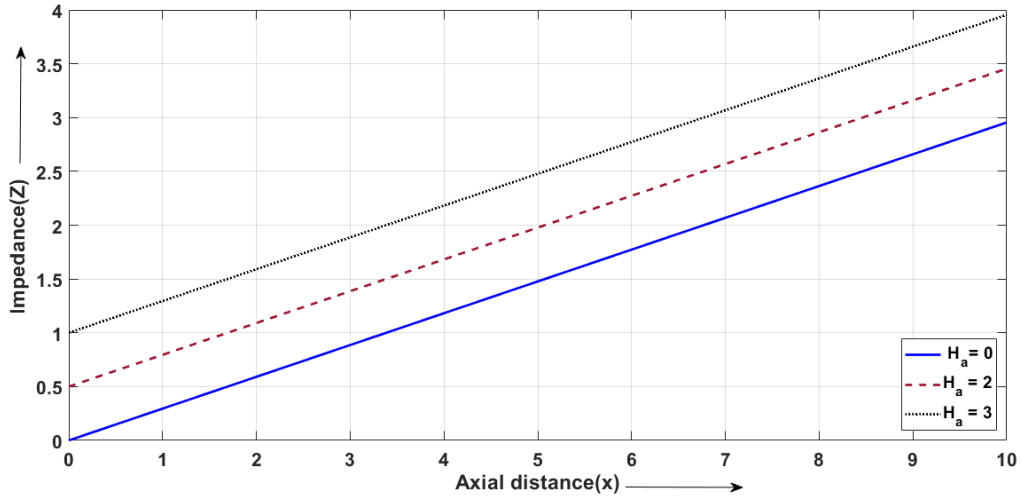

Figure 8: The effect of Hartmann number on impedance

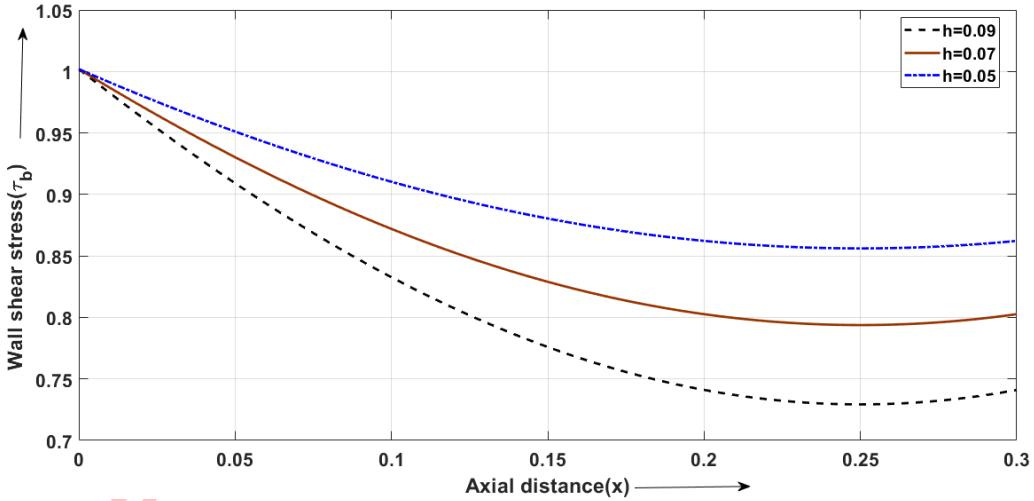

Figure 9: The effect of stenosis height on wall shear stress

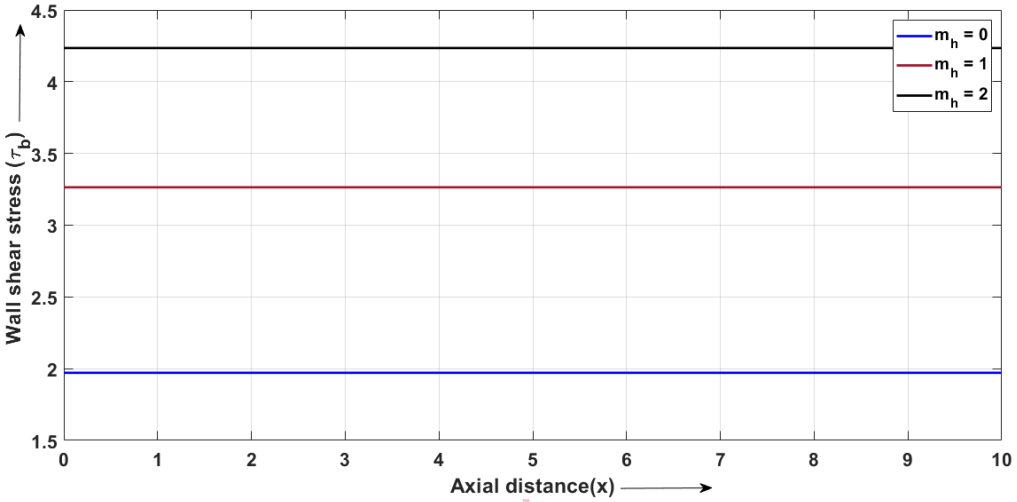

Figure 10: The effect of Hall parameter on wall shear stress

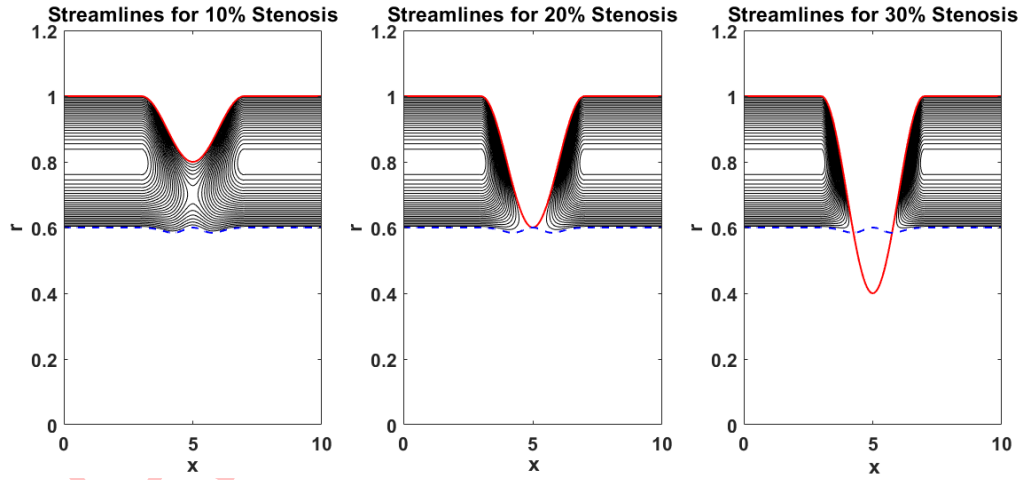

Figure 11: Streamline patterns for 10, 20, and 30% stenosis showing progressive flow acceleration and distortion as the degree of narrowing increases

4 Conclusion

The current study demonstrates blood and nanoparticle interactions within a stenosed artery are significantly impacted by magnetic, thermal, and flow parameters. Magnetic fields (utilizing the Hartmann and Hall effects) altered the velocity and flow through the artery of the selected stenosis, potentially allowing control of efficacy underlying targeted therapies. As an example, radiation efficiently cools the area, directly assisting with thermal regulation of the arteries while higher Schmidt numbers have improved concentration gradients thereby improving drug delivery for selected arteries. Higher impedance reflects the strength of magnetic opposition and variability in wall shear stress demonstrates elevated risk of stenosis severity and involvement. These implications support a pathway towards in-situ design of magnetic drug delivery systems, development of diagnostic tools, and management of vascular diseases with the establishment of these theoretical foundations.

Acknowledgements

The authors thank the university for providing the necessary software, laboratory, and other academic facilities that supported this research.

Conflict of Interest

The authors declare that there are no conflicts of interest regarding the publication of this paper.

Funding

This research did not receive any specific grant from funding agencies in the public, commercial, or not-for-profit sectors.

Appendix 1

$$\beta_1 = \left(\frac{K_0 R_d^2}{\gamma_b^2} + i\omega \frac{P_e}{\mathbf{d}_b}\frac{K_0}{s_0}\right), \quad \beta_2 = \left(R_d^2 + i\omega P_e\right), \qquad \xi_1 = i\omega R_{ey} D_b S_c, \quad \xi_2 = i\omega R_{ey} S_c.$$

$$\lambda_1 = \left(H_a^2 + \frac{R_{ey}}{\mathbf{d}_b} i\omega\right)\mu_b, \qquad \lambda_2 = \left(\frac{H_a^2}{1+m_h^2} + R_{ey} i\omega\right).$$

$$V_1 = \frac{J_0(\sqrt{\beta_2}R_c)}{J_0(\sqrt{\beta_1}R_c)} - \frac{J_0(\sqrt{\beta_2}R_p)Y_0(\sqrt{\beta_2}R_c)}{Y_0(\sqrt{\beta_2}R_p)J_0(\sqrt{\beta_1}R_c)},$$

$$V_2 = \frac{Y_0(\sqrt{\beta_2}R_c)}{J_0(\sqrt{\beta_1}R_c)Y_0(\sqrt{\beta_2}R_p)}, \quad V_3 = \sqrt{\beta_1}V_1 J_1(\sqrt{\beta_1}R_c) - \sqrt{\beta_2}\left[J_1(\sqrt{\beta_2}R_c) - \frac{J_0(\sqrt{\beta_2}R_p)}{Y_0(\sqrt{\beta_2}R_p)}Y_1(\sqrt{\beta_2}R_c)\right],$$

$$V_4 = \frac{J_0(\sqrt{\xi_2}R_c)}{J_0(\sqrt{\xi_1}R_c)} - \frac{J_0(\sqrt{\xi_2}R_p)Y_0(\sqrt{\xi_2}R_c)}{Y_0(\sqrt{\xi_2}R_p)J_0(\sqrt{\xi_1}R_c)},$$

$$V_5 = \frac{Y_0(\sqrt{\xi_2}R_c)}{J_0(\sqrt{\xi_1}R_c)Y_0(\sqrt{\xi_2}R_p)}, \quad V_6 = \sqrt{\xi_1}V_5 J_1(\sqrt{\xi_1}R_c) - \sqrt{\xi_2}\left[J_1(\sqrt{\xi_2}R_c) - \frac{J_0(\sqrt{\xi_2}R_p)}{Y_0(\sqrt{\xi_2}R_p)}Y_1(\sqrt{\xi_2}R_c)\right].$$

Variation of Parameters Constants

$$A_1 = -\frac{\pi r}{2}\int Y_0(\sqrt{\lambda_1}r)P_0\mu_b\,dr, \quad B_1 = \frac{\pi r}{2}\int J_0(\sqrt{\lambda_1}r)P_0\mu_b\,dr,$$

$$A_2 = -\frac{\pi r}{2}\int Y_0(\sqrt{\lambda_2}r)P_0\,dr, \quad B_2 = \frac{\pi r}{2}\int J_0(\sqrt{\lambda_2}r)P_0\,dr.$$

$$C_1 = \frac{\frac{P_0}{\beta^2}\left(1 - \frac{J_0(\beta R_c)}{J_0(\beta R_p)}\right) + C_4\left[Y_0(\beta R_c) - \frac{J_0(\beta R_c)Y_0(\beta R_p)}{J_0(\beta R_p)}\right]}{J_0(\sqrt{\lambda_1}R_c)},$$

$$C_2 = 0,$$

$$C_3 = \frac{-\frac{P_0}{\beta^2} - C_4 Y_0(\beta R_p)}{J_0(\beta R_p)},$$

$$C_4 = \frac{\mu_c C_1\sqrt{\lambda_1}J_1(\sqrt{\lambda_1}R_c) + \mu_p\frac{P_0}{\beta}\frac{J_1(\beta R_c)}{J_0(\beta R_p)}}{\mu_p\beta\left[Y_1(\beta R_c) - \frac{J_1(\beta R_c)Y_0(\beta R_p)}{J_0(\beta R_p)}\right]}.$$

Here, J_0 and Y_0 denote Bessel functions of the first and second kind of order zero.

References

[1] S.K. Agarwal and H.V. Harsh, *Steady laminar boundary layer flow and heat transfer along an infinite, porous, hot, vertical moving plate in presence of heat source and constant free stream*, J. Rajasthan Acad. Phys. Sci. **16(3&4)** (2017) 155–166.

[2] M. Amkadni, A. Azzouzi and Z. Hammouch, *On the exact solutions of laminar MHD flow over a stretching flat plate*, Commun. Nonlinear Sci. Numer. Simulat. **13(2)** (2008) 359–368.

[3] R. Ellahi, S.U. Rahman, M.M. Gulzar, S. Nadeem and K. Vafai, *A mathematical study of non-Newtonian micropolar fluid in arterial blood flow through composite stenosis*, Appl. Math. Inf. Sci. **8(4)** (2014) 1567–1573.

[4] A.E. Garcia and D.N. Riahi, *Two-phase blood flow and heat transfer in an inclined stenosed artery with or without a catheter*, Int. J. Fluid Mech. Res. **41(1)** (2014) 16–30.

[5] M.M. Ghalib, A.A. Zafar, M.B. Riaz, Z. Hammouch and K. Shabbir, *Analytical approach for the steady MHD conjugate viscous fluid flow in a porous medium with nonsingular fractional derivative*, Physica A: Stat. Mech. Appl. **554** (2020) 123941.

[6] Y. Haik, V. Pai and C.-J. Chen, *Apparent viscosity of human blood in a high static magnetic field*, J. Magn. Magn. Mater. **225** (2001) 180–186.

[7] R. Khandelwal and S.K. Agarwal, *Hagen-Poiseuille flow in circular cylinder when temperature is exponential and sinusoidal function of length*, Adv. Theory Nonlinear Anal. Appl. **5(4)** (2021) 467–481.

[8] A. Ogulu and T.M. Abbey, *Simulation of heat transfer on an oscillatory blood flow in an indented porous artery*, Int. Commun. Heat Mass Transf. **32(7)** (2005) 983–989.

[9] R. Ponalagusamy and R.T. Selvi, *Influence of magnetic field and heat transfer on two-phase fluid model for oscillatory blood flow in an arterial stenosis*, Meccanica **50** (2015) 927–943.

[10] D.S. Sankar and U. Lee, *Two-phase non-linear model for the flow through stenosed blood vessels*, J. Mech. Sci. Technol. **21** (2007) 678–689.

[11] G. Sethi and S.K. Agarwal, *Analytic approach to non-Newtonian Jeffery fluid flow in a catheterized curved artery: Exploring the impact of heat, mass transfer and magnetic field*, Commun. Adv. Math. Sci. **8(2)** (2025) 86–99.

[12] S. Sharma, U. Singh and V.K. Katiyar, *Magnetic field effect on flow parameters of blood along with magnetic particles in a cylindrical tube*, J. Magn. Magn. Mater. **377** (2015) 395–401.

[13] J.K. Singh, S. Kolasani and G.S. Seth, *Scrutiny of induced magnetic field and Hall current impacts on transient hydromagnetic nanofluid flow within two vertical alternative magnetized surfaces*, Proc. Inst. Mech. Eng. E: J. Process Mech. Eng. **237(4)** (2023) 595–1606.

[14] J.K. Singh and S. Kolasani, *Energy dissipation and Hall effect on MHD convective flow of nanofluid within an asymmetric channel with arbitrary wall thickness and conductance*, Eur. Phys. J. Plus **136** 1074 (2021).

[15] J.K. Singh, Hanumantha and G.S. Seth, *Scrutiny of convective MHD second-grade fluid flow within two alternatively conducting vertical surfaces with Hall current and induced magnetic field*, Heat Transf. **51**(8) (2022).

[16] J.K. Singh, Hanumantha, S. Kolasani and S.M. Hussain, *Exploration of heat and mass transport in oscillatory hydromagnetic nanofluid flow within two verticals alternatively conducting surfaces*, Z. Angew. Math. Mech. (ZAMM) (2023).

[17] J.K. Singh, A. Kumar and A.K. Maurya, *Inspection of heat transport and magnetic induction in MHD second-grade hybrid nanofluid flow within a vertical channel with arbitrary conductive walls*, Int. J. Ambient Energy **46(1)** (2025).

[18] B. Tripathi and B.K. Sharma, *Influence of heat and mass transfer on MHD two-phase blood flow with radiation*, AIP Conf. Proc. **1975(1)** (2018) 030009.